



# Effect of porosity and interface structures on thermal and mechanical properties of SiC<sub>p</sub>/6061Al composites with high volume fraction of SiC

Yu HONG<sup>1</sup>, Wu-jie WANG<sup>2</sup>, Jia-qin LIU<sup>1,2,3</sup>, Wen-ming TANG<sup>1,4</sup>, Yu-cheng WU<sup>1,2,3,4</sup>

1. School of Materials Science and Engineering, Hefei University of Technology, Hefei 230009, China;
2. Institute of Industry & Equipment Technology, Hefei University of Technology, Hefei 230009, China;
3. Laboratory of Nonferrous Metal Material and Processing Engineering of Anhui Province, Hefei University of Technology, Hefei 230009, China;
4. National-Local Joint Engineering Research Centre of Nonferrous Metals and Processing Technology, Hefei University of Technology, Hefei 230009, China

Received 26 June 2018; accepted 7 January 2019

**Abstract:** 50 vol.% SiC<sub>p</sub>/Al composites with high thermal and mechanical properties were successfully produced by spark plasma sintering technique. The influences of sintering temperature on the thermal conductivity, coefficient of thermal expansion and bending strength of the SiC<sub>p</sub>/Al composites were carefully investigated. The results show that the SiC<sub>p</sub>/Al composites sintered at 520 °C exhibits a thermal conductivity of 189 W/(m·K), a coefficient of thermal expansion (50–200 °C) of  $10.03 \times 10^{-6} \text{ K}^{-1}$  and a bending strength of 649 MPa. The high thermal and mechanical properties can be ascribed to the nearly full density and the well interfacial bonding between the alloy matrix and the SiC particles. This work provides a promising pathway for producing materials to meet the needs of high performance electronic packaging.

**Key words:** spark plasma sintering; SiC<sub>p</sub>/6061Al composites; thermal properties; mechanical properties

## 1 Introduction

Effective heat dissipation has become more and more important for the reliability and life spans of semiconductor devices, due to continuously decreasing of the component size and increasing of the computer capability [1,2]. It is vital to develop thermal management materials with excellent thermal properties, such as high thermal conductivity (TC) [3,4], tailored coefficient of thermal expansion (CTE) [5] and low density [6]. Till now, several electronic packaging materials have been well studied, such as Cu–W [7], AlN [8], Al/diamond [1,5], and Al/SiC [9,10] composites. Among them, silicon carbide (SiC) particle dispersed Al-matrix composites with high ceramic content have drawn great attention for their extensive application prospect in advanced electronic packaging [11], owing to the excellent combination of attractive thermal and mechanical properties, such as low density, high thermal

conductivity, low coefficients of thermal expansion and high flexural strength.

Many preparation methods have been proposed to fabricate SiC<sub>p</sub>/Al composites with high volume fraction of SiC, such as pressureless infiltration [10], vacuum hot pressing [12], and powder metallurgy [13]. However, these methods have several shortages. For pressureless infiltration method, Al alloy with Si and/or Mg additions was used as matrix to avoid the formation of interfacial products (Al<sub>4</sub>C<sub>3</sub>), resulting in a detrimental influence on the thermal and mechanical properties of composites [11]. In addition, during the vacuum hot pressing process, the pores cannot be thoroughly eliminated at high temperature or the long holding time, pores considerably decrease the thermal conductivity of composites due to scattering of the heat flow [14].

In recent years, spark plasma sintering (SPS) methods have been adopted to SiC<sub>p</sub>/Al composites with high volume of SiC, which can reduce the formation of Al<sub>4</sub>C<sub>3</sub> at the interface effectively. TENG et al [13]

investigated the effect of SiC particles sizes and annealing on the thermo-mechanical of the 50 vol.% SiC<sub>p</sub>/Al composites. MIZUUCHI et al [5] studied thermal conductivity of SiC<sub>p</sub>/Al composites with monomodal and bimodal particle size distribution. The results demonstrated that the bimodal particle size distribution improved relative density and thermal conductivity of the composite. The reported literatures [15–20] demonstrate that SPS is a novel sintering technique to sinter SiC<sub>p</sub>/Al composites with well interfacial bonding and clean interface for short sintering and holding time at low temperatures. In addition, the spark discharge, Joule heating, and plastic deformation effects all contribute to densification of SiC<sub>p</sub>/Al composite during SPS process [21–27]. For a given Al alloy and the volume fraction of SiC particles, it is very likely that the thermo-mechanical properties of the SiC/Al composites prepared at various sintering temperatures are mainly attributed to the changes in the degree of densification and interfacial bonding. However, the influence of residual pore and interfacial bonding on thermo-mechanical properties of SiC/Al composites with high volume fraction of SiC has not been well studied.

Herein, the 50 vol.% SiC<sub>p</sub>/6061Al composites were fabricated by the SPS process, and the effects of the sintering temperature on the thermal and mechanical properties of the composites, such as thermal conductivity, coefficient of thermal expansion, and flexural strength, were systematically investigated for the fabrication of high performance electronic packaging materials.

## 2 Experimental

Atomized 6061Al alloy powders with a mean size of 8 μm and a purity of 99% were used as the matrix material, which exhibited nearly-spherical morphology. Green SiC particles with an average particle size of 16 μm and a purity of 99.5% were selected as the reinforcement. The 6061Al alloy powders were mixed with 50 vol.% SiC in a roller-mixer at a rotation speed of 180 r/min for 12 h, using zirconia balls as a milling medium. The mixed powders of SiC and 6061Al were compacted into the graphite die, and then sintered by a spark plasma sintering apparatus (LABOX–350, Sinter Land Inc., Nagaoka City, Japan). During the sintering process, the compacted bulk was heated to the preset temperature from 480 to 530 °C with a heating rate of 50 °C/min for 8 min of holding time in vacuum. The applied initial and holding compressive pressure levels were 30 and 50 MPa, respectively. The 6061Al alloy was sintered at 520 °C for performance comparison. The graphite die temperature was measured by thermocouple.

The sintered samples were about 25 mm in diameter and 5 mm in thickness. Before property characterization, the carbon diffusion layers were removed from the surfaces of the compacted bulks to avoid any contamination from conductive graphite paper. The sintered composites were cut into various sizes for characterization by using the wire cutting method. Particle size distribution of 6061Al alloy powder and SiC particles was measured by MS–2000 laser particle size analyzer. The microstructure of the sintered samples was characterized with a ZEISS Axio Lab. A1 type optical microscope. The reaction products on the fresh fracture surface of the samples were characterized using a D/max-rB type X-ray diffractometer (XRD, Cu K<sub>α</sub>, λ=0.1506 nm). The fractography of the sintered samples was observed with scanning electron microscope (SEM, Hitachi SU8020, Japan). Densities of the composites were calculated by using the Archimedes method. Thermal diffusivity of composite was measured based on the laser flash technique with a Netzsch LFA467 thermal constant analyzer. The sizes of the specimen for thermal conductivity testing were  $d12.7 \text{ mm} \times 3.5 \text{ mm}$ . Each thermal diffusivity value was the average value of four measurements to ensure the accuracy of the thermal diffusivity at room temperature. The specific heat capacity of the composite was derived from the theoretical value calculated based on rule of mixture (ROM) with the specific heat capacity of Al (0.88 J/(g·K)) and SiC (0.66 J/(g·K)). The thermal conductivity (TC, λ) of the composites was obtained from thermal diffusivity (α), density (ρ) and specific heat capacity (c<sub>p</sub>) according to the following equation [2]:

$$\lambda = \alpha \times \rho \times c_p \quad (1)$$

The coefficient of thermal expansion (CTE) of the composites (3 mm×4 mm×12 mm) was measured with a TMA402F3 type thermal mechanical analyzer in a N<sub>2</sub> flowing atmosphere in order to avoid oxidation of the sample from 25 to 200 °C at a heating rate of 2 °C/min. Three-points bending test was performed on a Shimadzu universal instrument with a testing span of 15 mm and a beam displacement rate of 0.5 mm/min, and the sizes of test samples were 3 mm × 4 mm × 22 mm.

## 3 Results and discussion

### 3.1 Morphology and microstructure characterization

Figure 1 shows the morphology and particle size distribution of 6061Al alloy powders and SiC particles, respectively. Figure 2 demonstrates the metallographic microstructures obtained from cross-sections of the SiC<sub>p</sub>/6061Al composites consolidated at different temperatures. During the sintering process, capillary force and the sintering pressure force the molten Al alloy

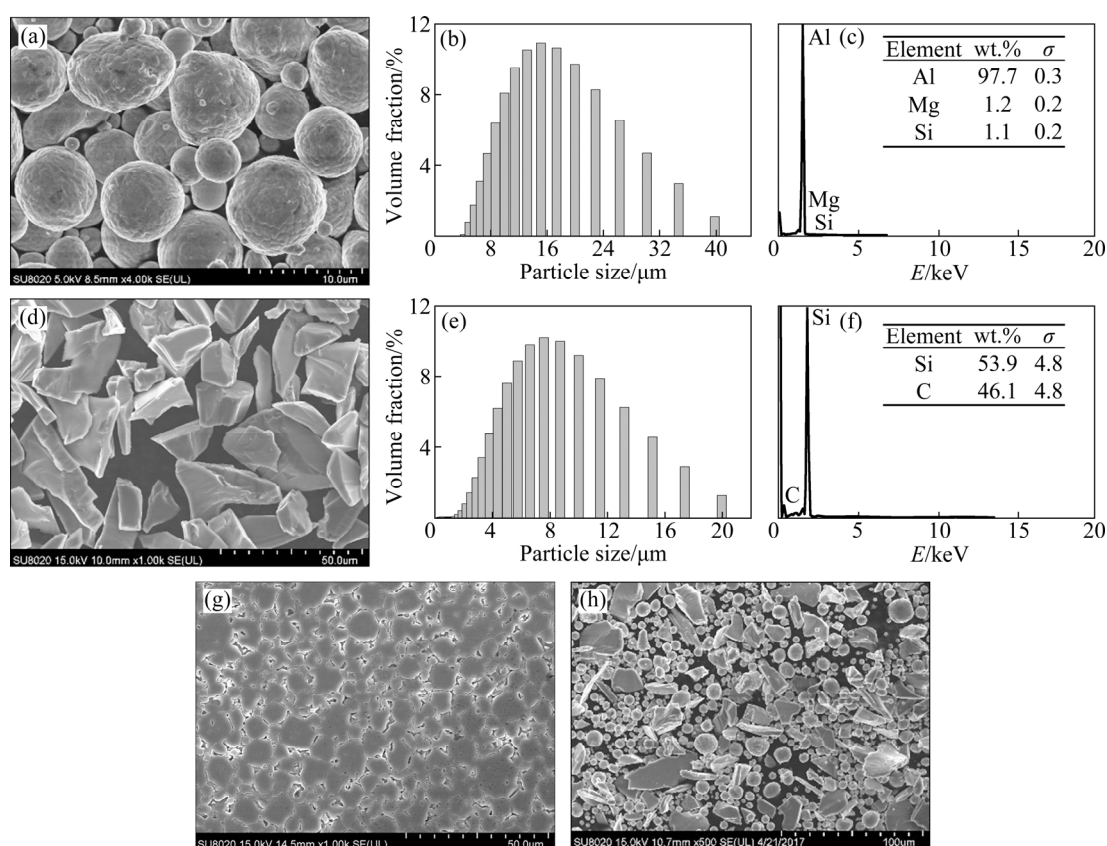


**Fig. 1** SEM image (a), particle size distribution (b), surface EDS analysis (c) of 6061Al alloy powders; SEM image (d), particle size (e), surface EDS analysis (f) of SiC particles; SEM image of mixed powder of 50 vol.% (SiC<sub>p</sub>+6061Al) (g), and microstructure of 6061Al alloy (h) ( $\sigma$  is the mean square error)

to infiltrate into the SiC particle gaps to achieve densification of the SiC<sub>p</sub>/6061Al composites. The metallographic microstructures of composites confirm the reduction of porosity with increasing temperature from 480 to 520 °C. For the composite sintered at 480 °C, the pores or cavities are observed obviously in the interfacial boundaries or among SiC particles as shown in Fig. 2(a), which could be ascribed to insufficient liquid phase filled gaps between particles during the sintering process. As shown in Fig. 2(e), with increasing the sintering process. As shown in Fig. 2(e), with increasing the temperature to 520 °C, it can be found that SiC particles are well dispersed and uniformly distributed in Al alloy matrix, and there is no evidence of pores or separated interface. On one hand, the solid-state diffusion between the SiC particles accelerated, and the molten Al alloy was obtained, which was beneficial to the interfacial bonding. On the other hand, the molten Al almost completely infiltrated into the gaps among SiC particles, which caused the densification of composites. So, the nearly full dense compaction was formed.

During the SPS process, high heating rates, especially in combination with short dwell times, can cause temperature gradients and subsequently sintering inhomogeneity leading to non-uniform microstructural

and mechanical properties of the sintered parts. VANMEENSEL et al [24] found that the temperature field of the conductive TiN sample gradually decreases from the center of the sample to the outer die wall surface and there is a greater radial temperature gradient. Therefore, when the temperature further increases to 530 °C, the high temperature in the center of the composite resulted from the spark discharge effect and the Joule heating may lead to the gasification of Al alloy, and the melted molten Al sprays out of the graphite die. As seen in Fig. 2(f), large pores can be observed at the internal of composite sintered at 530 °C, but other parts of the composites still maintain dense structure, which was different from that sintered at 480 °C.

### 3.2 Relative density and XRD patterns of composites at different sintering temperatures

The relative density of the composites sintered at 520 °C and graphite die temperature as a function of sintering time were investigated. As shown in Fig. 3, prior to SPS, the relative density is naturally low and remains unchanged until sintering temperature reaches about 180 °C, then it increases slowly with increasing sintering time. After that, the relative density increases

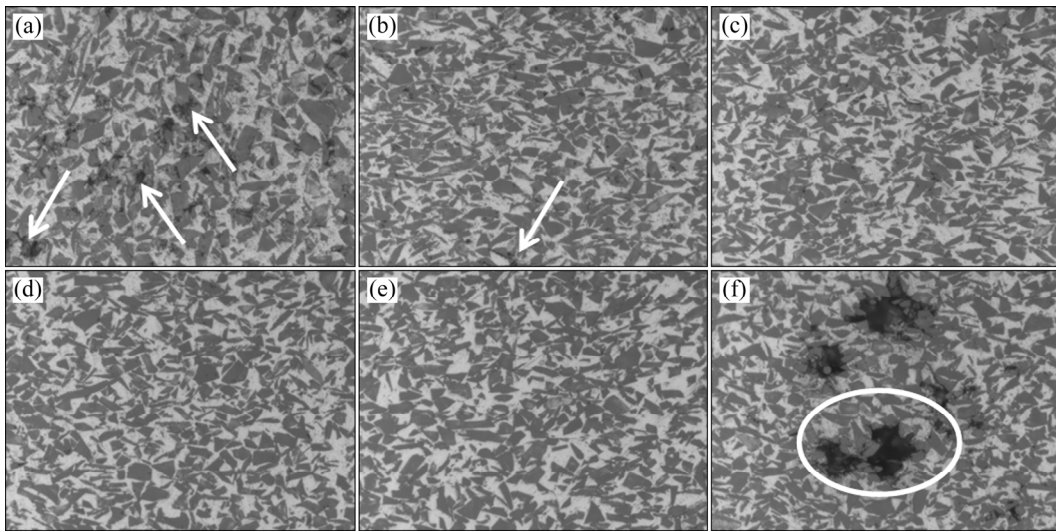


**Fig. 2** Metallographic microstructures of  $\text{SiC}_p/6061\text{Al}$  composites sintered at temperatures of 480 °C (a), 490 °C (b), 500 °C (c), 510 °C (d), 520 °C (e) and 530 °C (f)

abruptly with increasing temperature above 380 °C, which is considered to be caused by the melting of 6061Al alloy powder. It should be noted that the melting temperature of 6061Al alloy is far below melting point of 6061Al alloy, which can be attributed to the spark discharge effect and Joule heat during SPS processing. When the graphite die temperature rises to about 480 °C, the relative density reaches almost a plateau with further sintering. The large pores present in the sintered body are filled with molten 6061Al alloy. However, the small pores are hardly to be infiltrated at such a lower sintering pressure. Therefore, the relative density of the composite increases again with the increasing pressure from 30 to 50 MPa after the sintering temperature reaches the preset temperature, and it reaches higher than 99.8% of the theoretical density. For one thing, the solid-liquid co-existent state is very effective not only for rapid densification of  $\text{SiC}_p/\text{Al}$  composites, but also for producing strong bonding between the SiC particles and the Al alloy. For another, the displacement and

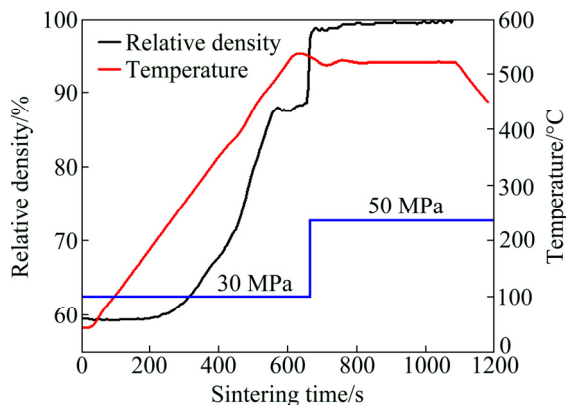


**Fig. 3** Relative density and graphite die temperature as function of sintering time during SPS process

rearrangement of SiC particles in the liquid phase further promote the densification of composites after increasing pressure from 30 to 50 MPa.

Figure 4 shows the relative density of  $\text{SiC}_p/6061\text{Al}$  composites with 50 vol.% SiC sintered at various temperatures. The plot reveals that the sintering temperature has a remarkable effect on the relative density of  $\text{SiC}_p/6061\text{Al}$  composites. With increasing sintering temperature from 480 to 500 °C, the relative density of the bulk compact increases from 92.18% to 99.15%, with much of densification occurring. As the sintering temperature exceeds 500 °C, the density continues to increase, but at a slower rate, which can be ascribed to incapability of being filled in the small amount of residual pores at much higher temperatures. However, when the sintering temperature rises to 530 °C, the partial seepage of Al results in the relative density drastically decreasing. And the relative density drops down to 95.91%, which is equivalent to that of the composite sintered at 490 °C.

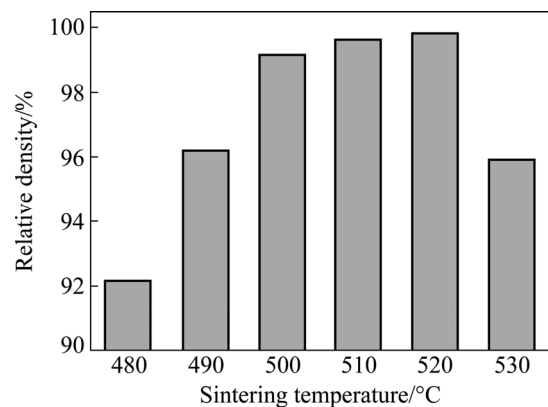


**Fig. 4** Relative density of  $\text{SiC}_p/6061\text{Al}$  composites sintered at different temperatures

Figure 5 shows the X-ray diffraction patterns of cross-sections of the SiC<sub>p</sub>/6061Al composites at different sintering temperatures. The SiC<sub>p</sub>/6061Al is composed of Al and SiC phases. The interface reaction products such as MgAl<sub>2</sub>O<sub>4</sub> and Al<sub>4</sub>C<sub>3</sub> have not been detected. In general, Al<sub>4</sub>C<sub>3</sub> is an undesirable intermetallic phase in electronic packing material because of its unstable and hygroscopic properties, which results in the degradation of thermal and mechanical properties of composites. This interface reaction (Eq. (2)) has been observed by many researchers [10,19,23].

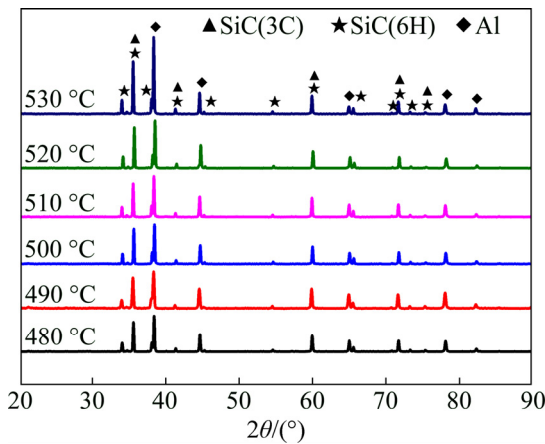
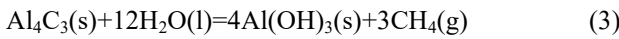
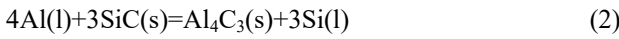


Fig. 5 X-ray diffraction patterns of SiC<sub>p</sub>/6061Al composites at different sintering temperatures

In the SPS process, formation of Al<sub>4</sub>C<sub>3</sub> during composite fabrication can be avoided effectively. This is mainly ascribed to the relatively short sintering process at low temperature [6], which is very beneficial to the prevention of Al<sub>4</sub>C<sub>3</sub> at the interface.

### 3.3 Thermal conductivity

Figure 6 presents the thermal conductivity (TC) of SiC<sub>p</sub>/6061Al composites as a function of the sintering temperature. The thermal conductivity of composites increases sharply when the sintering temperature is below 500 °C, and it increases at a slower rate with the sintering temperature increasing from 500 to 520 °C. However, the TC of the composites sintered at 530 °C drops to 139 W/(m·K), 26.5% lower than that sintered at 520 °C. In this work, for a given volume fraction of SiC, porosity and interfacial thermal conductivity in the composites are two important factors affecting the thermal conductivity of composite materials. In particular, the lower sintering temperature not only produces many porosities that will scatter phonons and electrons and have lower thermal conductivity of the inside air, but also leads to poor interfacial bonding

between the SiC particles and the Al matrix, which sacrifices heat transfer across the SiC–Al interfaces. Therefore, the SiC<sub>p</sub>/6061Al composite with low porosity and strong interfacial bonding is very important for pursuing high thermal property.

TC of the SiC<sub>p</sub>/6061Al composites sintered at various temperatures was theoretically analyzed by Two-Step Hasselman-Johnson (TS-HJ) model [28] proposed by MOLINA et al [29].

$$K_c = \frac{K_m[2K_m + K_p^{\text{eff}} + 2(K_p^{\text{eff}} - K_m)V_p]}{2K_m + K_p^{\text{eff}} - (K_p^{\text{eff}} - K_m)V_p} \quad (4)$$

$$K_p^{\text{eff}} = \frac{K_p^{\text{in}}}{1 + K_p^{\text{in}}/(ah_c)} \quad (5)$$

where subscripts c, m and p stand for the composites, the matrix and the reinforcement, respectively;  $K$ ,  $V$ ,  $a$  and  $h$  are the TC, the volume fraction of the reinforcement, average reinforcement size and the interface thermal conductance, respectively;  $K_p^{\text{in}}$  is the intrinsic TC of the reinforcement;  $K_p^{\text{eff}}$  is the effective TC of reinforcement considering the size of reinforcement and the interfacial thermal resistance.

When the porosity of composites is considered, the metal matrix with certain amount of residual pores constitutes an effective metal matrix that has an effective TC.  $K_m^{\text{eff}}$ , derived from the TS-HJ model by taking  $K_p^{\text{eff}} = 0$ , is

$$K_m^{\text{eff}} = \frac{K_m^{\text{in}}(1 - \xi')}{1 + 0.5\xi'} \quad (6)$$

where  $\xi'$  and  $K_m^{\text{in}}$  are the effective fraction of pores and the intrinsic TC of the metal matrix (in the case, 6061Al matrix, 180 W/(m·K)), respectively.

The effective fraction of pores,  $\xi'$ , in the effective matrix is given by

$$\xi' = \frac{\xi}{1 - V_p} \quad (7)$$

where  $\xi$  is the porosity, mainly presented in the metal matrix as non-thermally conducting inclusions.

The theoretical TC of composites was calculated from Eq. (4), with  $K_p^{\text{eff}}$ ,  $K_m$  and  $h_c$  of 330 W/(m·K), 180 W/(m·K) and 6.65 W/(m<sup>2</sup>·K), respectively. It should be noted that the value of  $h_c$ , 6.65 W/(m<sup>2</sup>·K), was measured by CHU et al [6]. The theoretical TC of 50 vol.% SiC<sub>p</sub>/6061Al composites predicted by the TS-HJ model is 191.5 W/(m·K). As shown in Fig. 6(a), the calculated TC of the SiC<sub>p</sub>/6061Al composites goes up by increasing sintering temperature from 480 to 520 °C, over 95% of theoretical predictions by the TS-HJ model when the sintering temperature is 520 °C, and then drops down sharply after sintering temperature is over 520 °C.

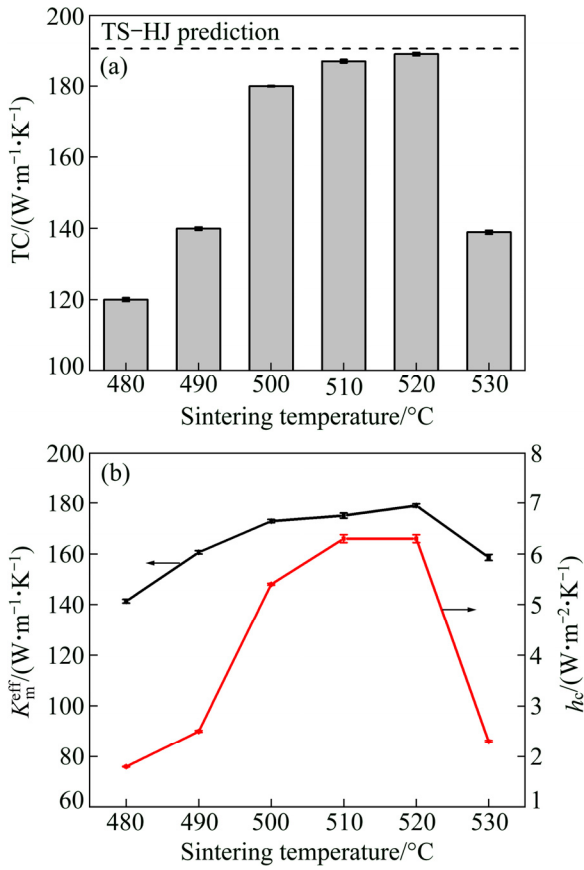


**Fig. 6** TC of SiC<sub>p</sub>/6061Al composites at different sintering temperatures (a) and effective TC of matrix ( $K_m^{eff}$ ) and interface conductance ( $h_c$ ) of SiC<sub>p</sub>/6061Al composites sintered at different sintering temperatures (b)

The interface thermal conductance,  $h_c$ , could be back-calculated from Eq. (5) by substituting  $K_m$  with  $K_m^{eff}$ , whereas the  $K_m^{eff}$  is calculated from Eq. (6) by first calculating  $\zeta'$  from Eq. (7). The calculated  $h_c$  goes up from 1.8 to 6.3  $W/(m^2 \cdot K)$  by increasing sintering temperature from 480 to 520  $^{\circ}C$  due to the enhanced interfacial bonding, and the  $K_m^{eff}$  grows from 141 to 179  $W/(m \cdot K)$  because of the reduction of the porosity, as shown in Fig. 2(c). Therefore, the TC enhancement of the SiC<sub>p</sub>/6061Al composites at sintering temperatures ranging from 480 to 520  $^{\circ}C$  can be ascribed to the reduction of the porosity and the improved interface conductance. However, with the sintering temperature increasing to 530  $^{\circ}C$ , the interface conductance shows a decline and it drops down to 2.3  $W/(m^2 \cdot K)$  probably due to the large pores in the center of the composite, observed by metallography in Fig. 2(f).

**3.4 Coefficient of thermal expansion**

The thermal expansion of the SiC<sub>p</sub>/6061Al composites is dependent on the thermal expansion of aluminum matrix, SiC, and the restriction of SiC particles through interfaces. TURNER [30] and

KERNER [31] have proposed models to theoretically predict the CTE of composites. TURNER model is based on the uniform hydrostatic stresses existing in the phase and composites can coordinate deformation. KERNER model takes account of normal shear stress at the boundaries between particles and the matrix. Hence, we utilized TURNER model and KERNER model to evaluate the CTE of composites. The two models can be expressed as Eqs. (8) and (9) as follows:

$$\alpha_c = \frac{\alpha_m V_m K_m + \alpha_d V_d K_d}{V_m K_m + V_d K_d} \tag{8}$$

$$\alpha_c = \alpha_m V_m + \alpha_d V_d + V_d V_m (\alpha_d - \alpha_m) \times \frac{K_d - K_m}{V_m K_m + V_d K_d + (3K_d K_m / 4G_m)} \tag{9}$$

where  $\alpha_c$ ,  $\alpha_m$  and  $\alpha_d$  are the CTE values of the composites, the matrix ( $24.0 \times 10^{-6} K^{-1}$  for Al) and the reinforcement ( $4.5 \times 10^{-6} K^{-1}$  for SiC), respectively;  $V_d$  and  $V_m$  stand for the volume fractions of the reinforcement and the matrix in the composites;  $K_d$  and  $K_m$  are the bulk moduli of volume fractions of the reinforcement ( $2.2 \times 10^{11}$  Pa for SiC) and the matrix ( $7.6 \times 10^{10}$  Pa for Al);  $G_m$  is the shear modulus of the matrix ( $2.6 \times 10^{10}$  Pa for Al).

The elongation of the composites changes with the test temperature. The average CTE of SiC<sub>p</sub>/6061Al composites and the theoretical data predicted by TURNER and KERNER models are shown in Fig. 7. The elongation of all composites increases with increasing test temperature, which could be ascribed to the increase of CTE of the matrix and the reduction of the restriction ability of SiC particles through interfaces. The average CTE of SiC<sub>p</sub>/6061Al composite between 20 and 200  $^{\circ}C$  is gradually approaching the TURNER theoretical predictions, indicating that the interfacial bonding becomes stronger as the sintering temperature increases from 480 to 520  $^{\circ}C$ , which helps to enhance the restriction on aluminum, thus reducing the CTE of the composite. LEMIEUX et al [32] have found that polygonal SiC particles would give a higher restriction on the matrix. The KERNER model indicates that the reinforcement is spherical particles, which leads to a higher CTE than the measured value. However, as the sintering temperature increases to 530  $^{\circ}C$ , the larger voids and poor interfacial bonding in the composite result in the significant increase of the coefficient of thermal expansion.

**3.5 Bending strength and fractography**

Figure 8 presents the influence of the sintering temperature on the bending strength of the SiC<sub>p</sub>/6061Al composites. The bending strength of the SiC<sub>p</sub>/6061Al composites sintered at 480  $^{\circ}C$  is 367 MPa. The relatively low level of densification and the lack of strong inter-

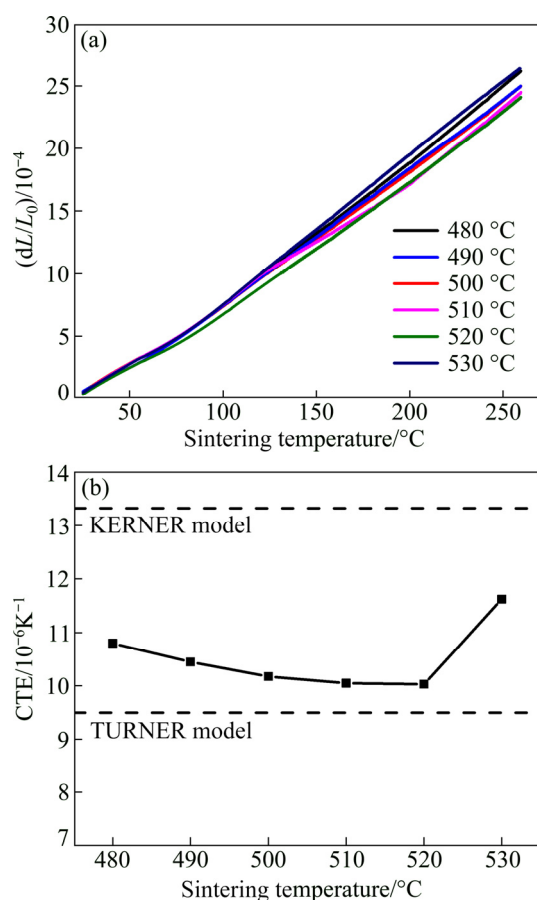


**Fig. 7** Elongation of  $\text{SiC}_p/6061\text{Al}$  composites at different sintering temperatures (a) and average CTE as function of testing temperature (b)

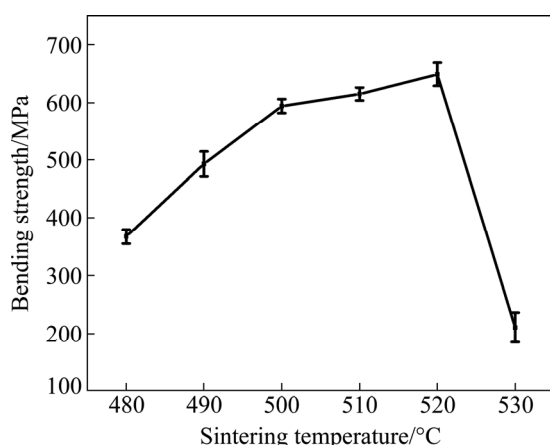


**Fig. 8** Bending strength of  $\text{SiC}_p/6061\text{Al}$  composites sintered at different temperatures

particle bonding of the sample fabricated at the sintering temperature of 480 °C lead to the lower bending strength [33]. Obviously, the bending strength increases rapidly when the sintering temperature is below 500 °C. Subsequently, the bending strength increases at a slower rate when further increasing the sintering temperature to 520 °C. The bending strength increases, which can be

ascribed to improved inter-particle adhesion and the matrix-reinforcement interfacial bonding with the sintering temperature increasing, and reaches its maximum of 649 MPa when sintered at 520 °C. When the sintering temperature extends to 530 °C, large pores can be detected at the center of the sintered compaction. Hence, the bending strength of the composite sintered at 530 °C drops down to 211 MPa, which is ever lower than that of the composite sintered at 480 °C.

Figure 9 shows the fracture micrographs of the composites sintered at different temperatures. In the  $\text{SiC}_p/6061\text{Al}$  composites, the critical criterion of the fracture mechanism of SiC particles (particle fracture or pull-out) is dependent on the relationship between the particle strength and the interface (SiC/Al) strength. If the particle strength is higher than Al/SiC interface strength, particle pull-out will be the predominant mode of fracture [34]. With the sintering temperature increasing, the interface bonding between the Al alloy and SiC particle gradually occurs and the composites are much more consolidated. For the  $\text{SiC}_p/6061\text{Al}$  composite sintered at 480 °C, the unburnt Al, interface debonding and many pores existing at the fracture of composites are observed in Fig. 8(a), indicating that the  $\text{SiC}_p/6061\text{Al}$  composites are not complete densification and have a poor interface bonding, which may cause poor interface conductance and weak bending strength. With the temperature increasing to 520 °C, local particle pull-out and pores on the fracture surface of composites are invisible. The cleavage fracture of SiC particles is tightly embedded in the ductile dimple of the Al alloy, as shown in Fig. 9(e). This indicates a strong interfacial bonding between Al matrix and the SiC particles, and sufficient load transfer from Al matrix to the SiC particles. Under the temperature up to 530 °C, large pores can be seen and a little Al adhered on the surface of SiC (Fig. 9(f)), mainly because of the improving flow-ability of the molten Al caused by the high local temperature and the partial seepage of Al under pressure.

## 4 Conclusions

(1) The XRD analysis results indicated that the phases of the composites sintered at temperature ranging from 480 to 530 °C only consist of SiC and Al.

(2) The composites fabricated by sintering at the temperature of 520 °C for 8 min under 50 MPa was sufficient for consolidation to achieve a nearly full density as well as good interfacial bonding with a relatively high TC, low CTE and high bending strength of 189 W/(m·K),  $10.03 \times 10^{-6} \text{ K}^{-1}$  and 649 MPa, respectively.

(3) Increasing the sintering temperature to 530 °C, the high temperature in the center of the compact

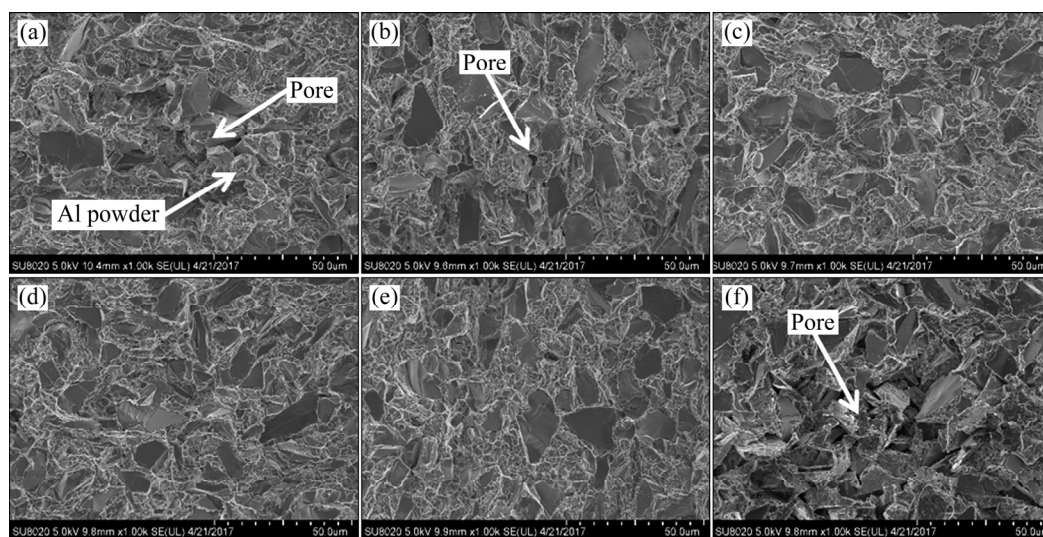


**Fig. 9** Fracture surface of SiC<sub>p</sub>/6061Al composites sintered at temperatures of 480 °C (a), 490 °C (b), 500 °C (c), 510 °C (d), 520 °C (e) and 530 °C (f)

resulting from the spark discharge effect may lead to the partial seepage of the Al alloy. As a result, the thermal and mechanical properties of the composite sintered at 530 °C severely decreased due to some large pores in the center of the compact and the weakness of the interface bonding.

## References

- [1] TAN Zhan-qiu, LI Zhi-qiang, FAN Gen-lian, KAI Xi-zhou, JI Gang, ZHANG Lan-ting, ZHANG Di. Fabrication of diamond/aluminum composites by vacuum hot pressing: Process optimization and thermal properties [J]. *Composites Part B: Engineering*, 2013, 47: 173–180.
- [2] YU J H, WANG C B, SHEN Q, ZHANG L M. Preparation and properties of Si<sub>p</sub>/Al composites by spark plasma sintering [J]. *Materials and Design*, 2012, 41: 198–202.
- [3] WANG Shi-ren, QIU Jing-jing. Enhancing thermal conductivity of glass fiber/polymer composites through carbon nanotubes incorporation [J]. *Composites Part B: Engineering*, 2010, 41(7): 533–536.
- [4] YOSHIDA K, MORIGAMI H. Thermal properties of diamond/copper composite material [J]. *Microelectronics Reliability*, 2004, 44(2): 303–308.
- [5] MIZUUCHI K, INOUE K, AGARI Y, SUGIOKA M, TANAKA M, TAKEUCHI T, TANI J, KAWAHARA M, MAKINO Y, ITO M. Bimodal and monomodal diamond particle effect on the thermal properties of diamond-particle-dispersed Al-matrix composite fabricated by SPS [J]. *Microelectronics Reliability*, 2014, 54(11): 2463–2470.
- [6] CHU Ke, JIA Cheng-chang, TIAN Wen-huai, LIANG Xue-bing, CHEN Hui, GUO Hong. Thermal conductivity of spark plasma sintering consolidated SiC<sub>p</sub>/Al composites containing pores: Numerical study and experimental validation [J]. *Composites Part A: Applied Science and Manufacturing*, 2010, 41(1): 161–167.
- [7] LORENTZEN T, CLARKE A P, POULSEN H F, GARBE S, GRAAFSMA H. Local strain contours around inclusions in wire-drawn CuW composites [J]. *Composites Part A: Applied Science and Manufacturing*, 1997, 28(7): 667–674.
- [8] YOSHIOKA T, MAKINO Y, MIYAKE S. Influence of phase change in intergranular oxides to thermal conductivity of AlN sintered by millimeter-wave heating [J]. *Journal of the Japan Society of Powder and Powder Metallurgy*, 2003, 50(11): 916–920.
- [9] XUE C, YU J K. Enhanced thermal transfer and bending strength of SiC/Al composite with controlled interfacial reaction [J]. *Materials and Design*, 2014, 53(1): 74–78.
- [10] WAND Dong-mei, ZHENG Zhi-xiang, LV Jun, XU Guang-qing, ZHOU Shi-ang, TANG Wen-ming, WU Yu-cheng. Enhanced thermal conductive 3D-SiC/Al-Si-Mg interpenetrating composites fabricated by pressureless infiltration [J]. *Ceramics International*, 2017, 43(2): 1755–1761.
- [11] MIZUUCHI K, INOUE K, AGARI Y, NAGAOKA T, SUGIOKA M, TANAKA M, TAKEUCHI T, TANI J, KAWAHARA M, MAKINO Y, ITO M. Processing of Al/SiC composites in continuous solid-liquid co-existent state by SPS and their thermal properties [J]. *Composites Part B: Engineering*, 2012, 43(4): 2012–2019.
- [12] SAHINER A, BEDIR F, YILMAZ N. Characteristic properties of Al-Cu-SiC<sub>p</sub> and Al-Cu-B<sub>4</sub>C<sub>p</sub> composites produced by hot pressing method under nitrogen atmosphere [J]. *Materials and Design*, 2007, 28(4): 1238–1244.
- [13] TENG Fei, YU Kun, LUO Jie, FANG Hong-jie, SHI Chun-li, DAI Yi-long, XIONG Han-qing. Microstructures and properties of Al-50%SiC composites for electronic packaging applications [J]. *Transactions of Nonferrous Metals Society of China*, 2016, 26(10): 2647–2652.
- [14] KUMARI L, ZHANG T, DU G H, LI W Z, WANG Q W, DATYE A, WU K H. Thermal properties of CNT-Alumina nanocomposites [J]. *Composites Science and Technology*, 2008, 68(9): 2178–2183.
- [15] DASH K, CHAIRA D, RAY B C. Synthesis and characterization of aluminium-alumina micro- and nano-composites by spark plasma sintering [J]. *Materials Research Bulletin*, 2013, 48(7): 2535–2542.
- [16] ELDESOUKY A, JOHNSON M, SVENGREN H, ATTALLAH M M, SALEM H G. Effect of grain size reduction of AA2124 aluminum alloy power compacted by spark plasma sintering [J]. *Journal of Alloys and Compounds*. 2014, 609: 215–221.
- [17] WU Chuan-dong, FANG Pan, LUO Guo-qiang, CHEN Fei, SHEN Qiang, ZHANG Lian-meng, ENRIQUE J L. Effect of plasma activated sintering parameters on microstructure and mechanical properties of Al-7075/B<sub>4</sub>C composites [J]. *Journal of Alloys and Compounds*, 2014, 615: 276–282.

- [18] AKIN I, HOTTA M, SAHIN F C, YUCEL O, GOLLER G, GOTO T. Microstructure and densification of ZrB<sub>2</sub>-SiC composites prepared by spark plasma sintering [J]. Journal of the European Ceramic Society, 2009, 29(11): 2379–2385.
- [19] LIU Pei, WANG Ai-qin, XIE Jing-pei, HAO Shi-ming. Characterization and evaluation of interface in SiC<sub>p</sub>/Al composite [J]. Transactions of Nonferrous Metals Society of China, 2015, 25(5): 1410–1418.
- [20] HUANG Dan, CHEN Wei-ping, ZHANG Shao-yang, HE Zeng-xian. Dry friction and wear performance of SiC 3D continuous ceramic frame reinforced 7075Al alloy [J]. Transactions of Nonferrous Metals Society of China, 2010, 20(1): 54–58.
- [21] MEIR S, KALABUKHOV S, FROUMIN N, DARIEL M P, FRAGE N. Synthesis and densification of transparent magnesium aluminate spinel by SPS processing [J]. Journal of the American Ceramic Society, 2009, 92(2): 358–364.
- [22] KIM G S, SHIN D H, SEO Y I, KIM Y D. Microstructure and mechanical properties of a ZnS-SiO<sub>2</sub> composite prepared by ball-milling and spark plasma sintering [J]. Materials Characterization, 2008, 59(9): 1201–1205.
- [23] ZHANG Zhao-hui, WANG Fu-chi, LUO Jie, LEE Shu-kui, WANG Lu. Microstructures and mechanical properties of spark plasma sintered Al-SiC composites containing high volume fraction of SiC [J]. Materials Science and Engineering A, 2010, 527(27–28): 7235–7240.
- [24] VANMEENSEL K, LAPTEV A, HENNICKE J, VLEUGELS J, OVD B. Modelling of the temperature distribution during field assisted sintering [J]. Acta Materialia, 2005, 53(16): 4379–4388.
- [25] YIN Fa-zhang, GUO Hong, JIA Cheng-chang, ZHANG Xi-min, ZHANG Yong-zhong. High thermal conductivity SiC<sub>p</sub>/Al electronic packaging materials by spark plasma sintering [J]. Acta Materialia Sinica, 2010, 27(1): 57–61.
- [26] ZENG Jing, PENG Chao-qun, WANG Ri-chu, WANG Xiao-feng. Research and development of metal matrix composites for electronic packaging [J]. The Chinese Journal of Nonferrous Metals, 2015, 25(12): 3255–3270. (in Chinese)
- [27] MAO Xue-zhi, HONG Yu, WANG Bin-hao, LIU Jun-wu, ZHANG Yu-jun, FENG Dong, YANG Lei, SHI Chang-dong, WU Yu-cheng, TANG Wen-ming. Fabrication, microstructures and properties of 50 vol.-% SiC<sub>p</sub>/6061Al composites via a pressureless sintering technique [J]. Powder Metallurgy, 2017(9): 1–9.
- [28] LYNCH J F, SPINDEL R C, SANG C C, MILLER J H, BIRDSALL T G. Results from the 1984 Marginal Ice Zone Experiment preliminary tomography transmissions: Implications for marginal ice zone, Arctic, and surface wave tomography [J]. Journal of Composite Materials, 1987, 21: 508–515
- [29] MOLINA J M, PRIETO R, NARCISO J, LOUIS E. The effect of porosity on the thermal conductivity of Al-12wt.% Si/SiC composites [J]. Scripta Mater, 2009, 60: 582–585.
- [30] TURNER P S. Thermal expansion stresses in reinforced plastics [J]. Journal of Research of the National Bureau of Standards, 1946, 37: 239–250.
- [31] KERNER E H. The elastic and thermo-elastic properties of composite media [J]. Proceedings of the Physical Society: Section B, 1956, 69: 808–813.
- [32] LEMIEUX S, ELOMARI S, NEMES J A, SKIBO M D. Thermal expansion of isotropic duralcan metal-matrix composites [J]. Journal of Materials Science, 1998, 33(17): 4381–4387.
- [33] SANCHEZ J M, ALVAREZ M, RODRIGUEZ N, ARISTIZABAL M. Effect of Ni powder characteristics on the consolidation of ultrafine TiMoCN cermets by means of SPS and HIP technologies [J]. Materials Science and Engineering A, 2009, 500(1–2): 225–232.
- [34] SHEN Y L, WILLIAMS J J, PIOTROWSKI G, CHAWLA N, GUO Y L. Correlation between tensile and indentation behavior of particle-reinforced metal matrix composites: an experimental and numerical study [J]. Acta Materialia, 2001, 49(16): 3219–3229.

## 孔隙率与界面结构对高体积分数 SiC<sub>p</sub>/Al 复合材料热学和力学性能的影响

洪雨<sup>1</sup>, 王武杰<sup>2</sup>, 刘家琴<sup>1,2,3</sup>, 汤文明<sup>1,4</sup>, 吴玉程<sup>1,2,3,4</sup>

1. 合肥工业大学 材料科学与工程学院, 合肥 230009;
2. 合肥工业大学 工业与装备技术研究院, 合肥 230009;
3. 合肥工业大学 安徽省有色金属材料与加工工程实验室, 合肥 230009;
4. 合肥工业大学 有色金属与加工技术国家地方联合工程研究中心, 合肥 230009

**摘要:** 采用放电等离子烧结技术成功制备具有高热学和力学性能的 50 vol.%SiC<sub>p</sub>/Al 复合材料, 研究烧结温度对复合材料热导率、热膨胀系数和抗弯强度的影响。结果表明, 在 520 °C 下烧结获得的复合材料, 导热系数为 189 W/(m·K), 热膨胀系数(50–200 °C)为 10.03×10<sup>-6</sup> K<sup>-1</sup>, 抗弯强度为 649 MPa。Al 合金基体与 SiC 颗粒之间的界面结合良好, 复合材料接近完全致密, 因而具有较高的热学性能和力学性能。为满足高性能电子封装材料的制备提供一种新的可行方法。

**关键词:** 放电等离子烧结; SiC<sub>p</sub>/6061Al 复合材料; 热学性能; 力学性能

(Edited by Xiang-qun LI)